Analysis of soliton pattern formation in passively mode-locked fiber lasers

A. Haboucha, H. Leblond, M. Salhi, A. Komarov,* and F. Sanchez
Laboratoire POMA, UMR 6136, Université d'Angers, 2 Bd Lavoisier, 49000 Angers, France
(Received 18 April 2008; published 6 October 2008)

We give a detailed theoretical analysis of spontaneous periodic pattern formation in fiber lasers. The pattern consists of a bound state of hundreds of pulses in a ring fiber laser passively mode locked by nonlinear rotation of the polarization. The phenomenon is described theoretically using a multiscale approach to the gain dynamics: the fast evolution of a small excess of gain is responsible for the stabilization of a periodic pattern, while the slow evolution of the mean value of gain explains the finite length of the quasiperiodic soliton train. The resulting model is well adapted to experimental observations in a Er:Yb-doped double-clad fiber laser.

DOI: 10.1103/PhysRevA.78.043806 PACS number(s): 42.55.Wd, 42.65.Tg, 05.45.Yv

I. INTRODUCTION

Soliton interaction is a fascinating subject of investigation because it can generate a large number of dynamical behaviors. Indeed, interacting solitons can lead, under some specific conditions, to the formation of a bound state which consists of two or more identical solitons with a constant phase difference between neighboring pulses. The investigation of bound states of nonconservative solitons was started about ten years ago with the theoretical prediction of the existence of a two-pulse bound state in the frame of the complex Ginzburg-Landau (CGL) equation [1–3]. Such an equation is universal in the sense that it can be applied to very different situations with a suitable choice of coefficients. In particular, it is well adapted to fiber lasers which support dissipative solitons. As a consequence, passively mode-locked fiber lasers have been good candidates for experimental confirmation of the existence of bound states. Experimental demonstration of such states was done a few years later in both normal and anomalous dispersion regimes in fiber lasers passively mode locked using the nonlinear polarization rotation technique [4–6]. Three- and four-pulse bound states have been also predicted [3,7] and observed [8–10]. However, both theoretical predictions and experimental observations are also limited to a few pulses [11].

On the other hand, indefinitely long periodic (conservative) soliton trains in one-dimensional Kerr media have been described theoretically and experimentally. These trains are formed due to the modulational instability of a continuous (cw) signal. These are not stationary states, since the cw signal is expected to be restored by the so-called Fermi-Pasta-Ulam (FPU) recurrence [12]. An analytical solution of the nonlinear Schrödinger (NLS) equation, which accounts for this phenomenon, has been found [13]. Experiments have been performed for both spatial [14] and temporal [15] solitons. An attempt to stabilize the array leads to the suppression of interactions between solitons [16]. In passive optical resonators, the stabilization of a periodic soliton train has been achieved, yielding a "soliton crystal" [17,18]. Infinite trains of dissipative solitons have been also experimentally demonstrated in erbium-doped fiber lasers and attributed to self-induced modulational instability [19,20]. More recently, the case of a high-repetition rate of fiber lasers has been revisited in terms of degenerate four-wave mixing [21]. Many experimental setups include Fabry-Perot filters to efficiently stabilize the train of pulses. In [21] the dynamics has been modeled with a phenomenological cubic Ginzburg-Landau equation.

This paper is devoted to a deep theoretical investigation of the formation of a bound state with a very large number of solitons. It is based on the experimental observation of a very long soliton train in a fiber laser [22], which is stable and phase locked as bound solitons and almost periodic as a soliton crystal. In addition, the soliton train has a finite length, very large with respect to the soliton size, but small with respect to the cavity length. This paper is organized as follows. In Sec. II, we briefly recall the experimental results obtained with a passively mode-locked erbium-doped fiber laser. A multiscale analysis is performed of the gain dynamics in Sec. III. This allows us to extract the fast component of the gain dynamics on the time scale of a pulse and the slow component on the time scale of the cavity round-trip time. The fast component is then used in Sec. IV to derive a master equation for pulse formation. We use an approach which has been used successfully in our previous works [23–26]. The final form of the model is a cubic complex Ginzburg-Landau equation with an integral term accounting for the fast gain dynamics and with coefficients which are related to physical parameters. In Sec. V we investigate numerically the formation of a periodic train of bound solitons starting from a normalized form of the master equation. It is demonstrated that the pulse separation and amplitude are defined by the parameters of the cavity. By means of an analytical single-pulse solution of the master equation, we calculate in Sec. VI the gain depletion resulting from the emergence of a pulse train. Finally the obtained value of the gain depletion is compared to the gain recovered through the pumping and a theoretical number of pulses in the train can be evaluated. We give several set of values of the orientation angles of the phase plates compatible with the existence of pulse trains of hundreds of solitons, in good agreement with experimental observations.

*Permanent adress: Institute of Automation and Electrometry, Russian Academy of Sciences, Acad. Koptyug Pr. 1, 630090 Novosibirsk, Russia.

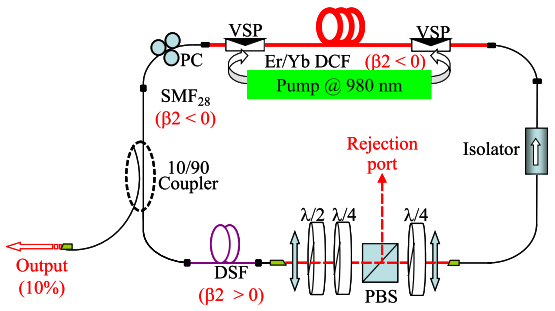

FIG. 1. (Color online) Experimental setup (PBS, polarization beam splitter; VSP, V-grooove side pumping; PC, polarization control).

II. EXPERIMENTAL RESULTS

In this section we briefly recall the experimental observations obtained with an Er:Yb-doped double-clad fiber laser in a unidirectional ring cavity and passively mode locked through nonlinear rotation of the polarization [22].

A. Experimental setup

The experimental arrangement is schematically represented in Fig. 1. It consists of a unidirectional ring cavity operating at 1.55 μm in which the mode locking is achieved thanks to the combined action of nonlinear polarization rotation, resulting from the optical Kerr effect, and an intracavity polarizer, which leads to fast intensity-dependent losses. The active fiber is a Er:Yb-doped double-clad fiber. The double-clad fiber consists of a single-mode core doped with ytterbium (for the pumping) and erbium ions and two clad. The large inner cladding allows a multimode propagation of the pump beam, thus allowing one to use compact high-power semiconductor lasers for the optical pumping. In addition, the inner cladding has a flower shape in order to break the cylindrical symmetry and then to efficiently increase the pump absorption coefficient. Two semiconductor laser diodes emitting at 980 nm are used in counterpropagating configuration; both have an available output power of about 3.5 W. The V-groove technique is employed to launch light into the fiber [27]. This technique allows us to let the fiber ends free and is then well adapted to ring laser cavities. An independent-polarization optical isolator is used to obtain unidirectional oscillation. The double-clad fiber (DCF) is 9 m long and has a group velocity dispersion (GVD) of $\beta_2 = -0.015$ ps^2/m; the standard SMF$_{28}$ fiber has anomalous dispersion ($\beta_2 = -0.0217$ ps^2/m) and is 9.6 m long. In order to manage the total cavity dispersion, a piece (2.15 m long) of dispersion-shifted fiber (DSF, $\beta_2 = +0.14$ ps^2/m) is used. The different lengths are such that the laser operates in the anomalous dispersion regime $\beta_2 L_{tot} = -0.04$ ps^2 (soliton regime). The 10% arm of a 90:10 fiber coupler is used for the output. Three phase plates are also inserted in the cavity in order to control the nonlinear losses and then to change the operating regime of the laser. Indeed, a simple rotation of a phase plate allows us to observe different regimes such as continuous, Q-switch, regular mode-locking, multiple pulsing, etc., regimes [28,29]. Depending on the parameter under

(a)

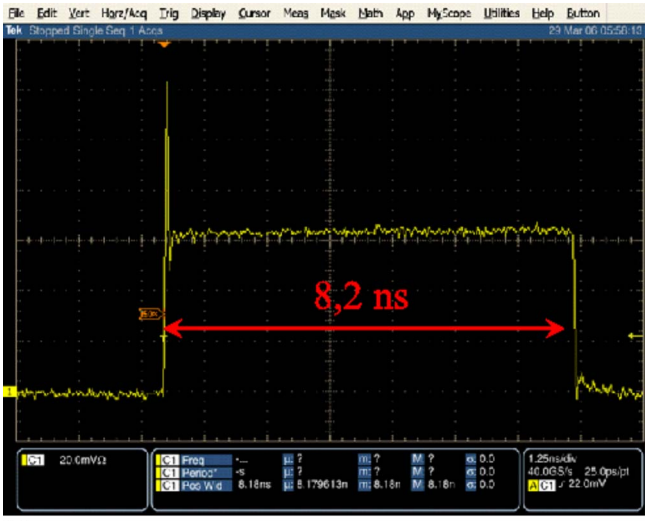

(b)

FIG. 2. (Color online) Oscilloscope trace: (a) the repetition of the pulse train at the fundamental frequency of the cavity and (b) the global shape of a train.

study, the analysis of the output signal is done with an optical spectrum analyzer (Anritsu MS 9710 C), an optical autocorrelator (Femtochrome FR-103 XL), a low-frequency spectrum analyzer (Rohde & Schwarz), or a fast single-shot oscilloscope with a bandwidth of 12 GHz (Tektronix TDS 61 124 C) associated with a fast optical detector (12 GHz) (Newport TIA-1200).

B. Bunch of locked pulses

As usual in fiber lasers with intracavity phase plates, their orientation allows the adjustment of the operating regime of the laser. For certain pumping rates and specific orientation of the phase plates, we observe pulse trains of several hundreds of pulses as shown in Fig. 2. The resolution of the fast detector and the oscilloscope is not sufficient to observe the detailed structure of the train. As a consequence, we observe a periodic square signal without internal structure. The pe-

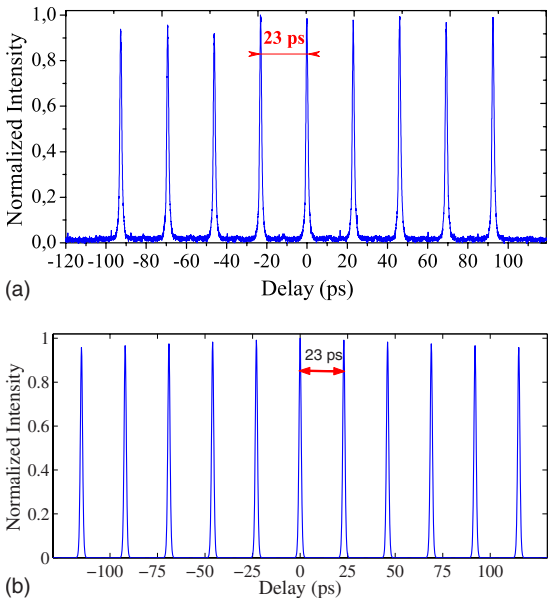

FIG. 3. (Color online) Autocorrelation trace showing the periodic local pattern: (a) experimental and (b) reconstructed.

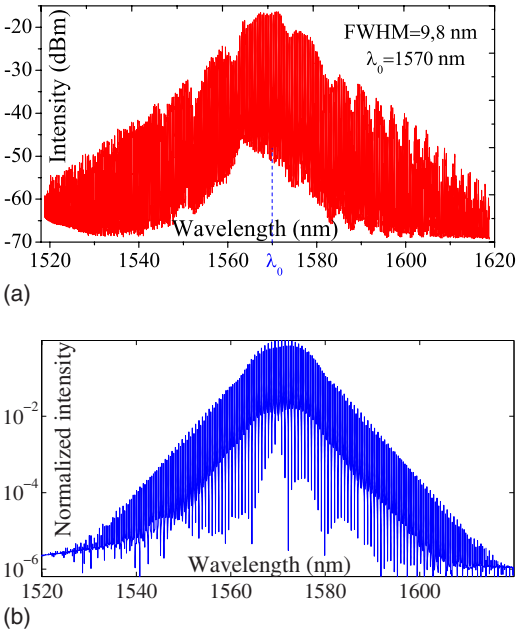

FIG. 4. (Color online) Optical spectrum of the pulse train: (a) experimental and (b) reconstructed.

riod of the signal coincides with the round-trip time of the cavity. The few oscillations that can be observed at the beginning of the square are not always present and are not significant. The autocorrelation trace given in Fig. 3 shows a local structure of periodic short pulses, but cannot show the whole train. In fact, for a set of some 100 bound pulses, the autocorrelation trace has a triangle envelope, but the center undergoes tiny variations, which cannot be detected in the experiment because they fall below the noise level of our detection. The sharpness of the peaks in the autocorrelation trace and the absence of a continuous component definitely prove the regularity of the periodic pattern. The optical spectrum reported in Fig. 4 exhibits a fast modulation which accounts for the periodic structure of the train and proves the mutual coherence between pulses; they interact and are phase locked. Recall that for a bunch state, where the pulses are not locked in phase, the optical spectrum is not modulated because it results from an averaging over thousands of round-trips. The spectrum of Fig. 4 also presents a global envelope that describes the soliton structure of the individual pulse.

C. Reconstruction

The pulse length is $\tau \simeq 900$ fs. The separation between pulses is $\Delta\tau = 23$ ps, as deduced from both the modulation of the spectrum and the autocorrelation trace. The total length is 8.2 ns and is found from the oscilloscope. This yields a number of pulses in the train of about $N = 350$. The interpretation of the spectrum and autocorrelation trace must be confirmed by a reconstruction from a given temporal shape. We use the ansatz

$$f = \sum_{j=1}^{N} E e^{i[\omega(t-j\Delta\tau)+j\delta\varphi]} \frac{e^{-iC(t-j\Delta\tau)^2/2\tau^2}}{\cosh\left(\frac{t-j\Delta\tau}{\tau}\right)}, \tag{1}$$

which includes a linear chirp with parameter C and a constant dephasing $\delta\varphi$ between two neighbor pulses. In the case of two bound pulses close together, the dephasing influences the shape of the spectrum, and consequently $\delta\varphi$ can be deduced from the latter [5]. However, in the present case, the separation between pulses is much larger, and hence the spectrum presents a very large number of of oscillations, which prevents such a determination. Thus $\delta\varphi$ cannot be determined experimentally, and its exact value is of very little importance for the reconstruction. It is arbitrarily taken as zero. The optical frequency is 193 THz. The simulation is restricted to a 100-pulse train due to limited computer memory. For a large number of pulses, its exact value only influences the width of the narrow peaks in the optical spectrum. This can be easily understood by a simple analogy with a classical diffraction grating: the greater the number of slits, the narrower the diffraction orders. The width of the spectrum indicates that a chirp is present; it is found that the best fit is obtained with a chirp parameter $C = 1.2$. The agreement in the spectrum (Fig. 4) and the autocorrelation trace (Fig. 3) demonstrates the validity of the above ansatz and estimated parameters.

As seen from the above analysis, several time scales are involved to account for the peak structure, the local periodical structure of the train, and the global finite length of the train, which is small with respect to the whole cavity length. Our theoretical approach will consider the behavior of the physical quantities as gain and electric field in the laser cavity at these different scales separately.

III. MULTISCALE ANALYSIS

In this section, a multiscale analysis is performed on the gain equation in order to account separately for its evolution at two time scales: The fast time scale governs the pulse formation, while the slow one is related to the duration of the train of pulses.

A. Gain dynamics

Erbium-doped fiber lasers pumped at 980 nm and operating at 1.55 μm can be considered as a quasi-four-level system [30]. The gain dynamics in a four-level model, assuming that the upper and lower nonradiative transitions are very fast (which allows the adiabatic elimination of the fast variables), is given by

$$\partial_t g = -\frac{g}{\tau_g} - ag\mathcal{P} + \Lambda, \tag{2}$$

where ∂_t is the derivative operator with respect to the time variable t, τ_g is the relaxation time, and the optical field power is $\mathcal{P}=A_{eff}I$, in which $A_{eff}\approx 70\ \mu\text{m}^2$ is the effective core area of the fiber. The saturation coefficient a can be expressed as $a=\sigma\tau_g/(h\nu A_{eff}T_{rt})$, where $\sigma=5\times10^{-25}\ \text{m}^2$ [30] is the cross section of the stimulated emission, $h\nu=13.26\times10^{-20}$ J is the energy of the photon with wavelength 1.55 μm, and $T_{rt}\approx 100$ ns is the cavity round-trip time.

The pumping coefficient is $\Lambda=\sigma R_p$, where the pumping rate R_p can be evaluated from experimental data using the equation [31]

$$R_p = \frac{\alpha_{lin}I_p}{h\nu_p}, \tag{3}$$

in which the pumping intensity I_p is assumed to be uniform along the fiber, $h\nu_p=2\times10^{-19}$ J is the energy of the pump photon with wavelength 980 nm, and $\alpha_{lin}=0.81\ \text{cm}^{-1}$ is the absorption coefficient of the pump. The regime under investigation is obtained for a pump power $P_p=3$ W, from which we deduce, using the cross section of the fiber cladding, $I_p=382\ \text{MW/m}^2$.

The relaxation time τ_g is about 10 ms, which is very large compared with the pulse duration (900 fs) or with the length of the pulse train (8.2 ns). The evolution of gain thus involves two very different time scales. It is characterized by a fast depletion, which follows the variations of the wave envelope, and a slow relaxation. The goal of the present section is to derive in a quite rigorous way two equations accounting separately for these two phenomena. This can be done by means of the multiscale expansion or reductive perturbation method [32].

Hence we introduce two time variables: a slow one τ, which will account for the relaxation, and a fast one T, which will account for the variations of the pulse envelope. Taking τ_g as a reference time, the slow time τ will coincide with the physical time t, and we introduce a small parameter η so that the fast time is $T=t/\eta$. The parameter η is typically the ratio of the pulse length to the relaxation time τ_g. The time derivative operator becomes

$$\partial_t = \frac{1}{\eta}\partial_T + \partial_\tau, \tag{4}$$

the gain is expanded in a power series of η as

$$g = g_0 + \eta g_1 + O(\eta^2), \tag{5}$$

and the expansion is inserted into Eq. (2). At leading order η^{-1}, it is found that $\partial_T g_0=0$; hence, g_0 depends on the slow variable τ only: the fast variations of the gain remain small.

At order η^0, we get

$$\partial_T g_1 + \partial_\tau g_0 = -\left(\frac{1}{\tau_g} + a\mathcal{P}\right)g_0 + \Lambda. \tag{6}$$

Equation (6) is integrated to yield

$$g_1(T,\tau) = (T-T_0)\left(-\partial_\tau g_0 - \frac{g_0}{\tau_g} + \Lambda\right) - ag_0\int_{T_0}^{T}\mathcal{P}(T',\tau)dT' + g_1(T_0,\tau), \tag{7}$$

T_0 being some initial time. Indeed, g_0 does not depend on T, and we assumed that the pumping parameter Λ also does, which is the case for constant pumping. The secular term in expression (7) of g_1 must vanish. More precisely, the correction g_1 must be sublinear—i.e., $\lim_{T\to+\infty}(g_1/T)=0$. This yields the condition

$$\frac{\partial g_0}{\partial\tau} = -\left(\frac{1}{\tau_g} + a\langle\mathcal{P}\rangle\right)g_0 + \Lambda, \tag{8}$$

where

$$\langle\mathcal{P}\rangle = \lim_{T\to+\infty}\frac{1}{T}\int_{T_0}^{T}\mathcal{P}(T',\tau)dT', \tag{9}$$

which depends on the slow time variable τ only. We let T_0 tend to $-\infty$; then, $\langle\mathcal{P}\rangle$ is the mean value of $\mathcal{P}$, averaged over all values of the fast variable T. Thus, as usual in multiscale expansions, the evolution law (8) of the leading term g_0 of the gain with respect to the slow variable τ is given by the nonsecularity condition for the evolution of the correction g_1 with respect to the fast variable T.

Setting $\Delta\mathcal{P}=\mathcal{P}-\langle\mathcal{P}\rangle$ and assuming that g_1 vanishes as T tend to $-\infty$, we get the expression of g_1 as

$$g_1 = -ag_0\int_{-\infty}^{T}\Delta\mathcal{P}(T')dT', \tag{10}$$

which accounts for the fast variations of the gain. Coming back to the laboratory coordinates, we obtain

$$g = g_0\left(1 - a\int_{-\infty}^{t}[\mathcal{P}(t') - \langle\mathcal{P}\rangle]dt'\right), \tag{11}$$

where $\langle\mathcal{P}\rangle$ is the mean value of the field power over one or a few round-trips.

B. Interpretation of the pulse train formation

The above analysis has evidenced two different time scales for the gain evolution: an immediate response to the perturbation induced by the pulse, which is expressed as an integral term, and a slow relaxation. The immediate response is expected to modify the propagation properties of the individual pulse and its interaction with its neighbors. At this scale, the structure of the pulse train is periodic. On the other hand, the whole pulse train has a finite length. At the time scale which characterizes this length, the variations of the average gain are not negligible anymore. Between two consecutive passes of the train, the gain evolution is governed by

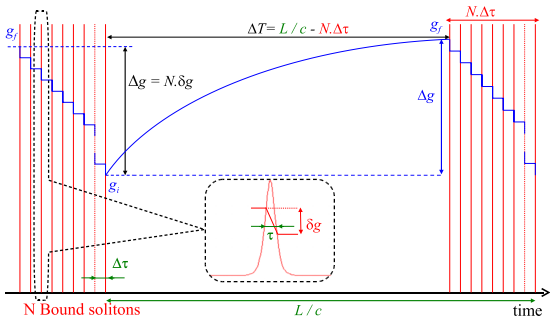

FIG. 5. (Color online) Evolution of the gain along the cavity: it is depleted by each pulse of the train and then restored by the pumping.

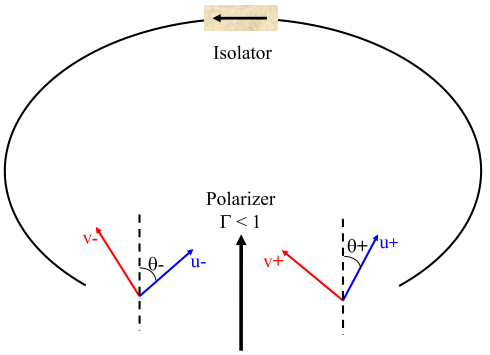

FIG. 6. (Color online) Orientation angles θ_- and θ_+.

relaxation and pumping, while a gain depletion occurs for each pulse and adds up over the whole train. The length of the train will be determined by the condition, which expresses the conservation of energy, that the depletion of the gain accumulated all along the train must be exactly compensated by the recovery of the gain due to the combined action of relaxation and pumping. This situation is illustrated in the Fig. 5.

IV. LOCAL BEHAVIOR: THE MEAN EVOLUTION EQUATION

The aim of this section is to derive a master equation for the electric field amplitude. A perturbative approach is performed on the propagation equations for the two polarization components of the electric field. The fast component of the gain dynamics is included in the initial equations. The electric field amplitude is then calculated just after the intracavity polarizer. This allows us to obtain a unique equation, thus greatly simplifying further analysis.

A. Propagation along the fiber

The nonlinear propagation of the envelope of the optical electric field components in the fiber is governed (in the fiber eigenaxis and in a frame moving at the group velocity) by the equations [23,33,34]

$$i\partial_z u - Ku - \frac{\beta_2}{2}\partial_t^2 u + \gamma(|u|^2 + A|v|^2 + Bv^2u^*) = ig\left(1 + \frac{1}{\omega_g^2}\partial_t^2\right)u, \tag{12}$$

$$i\partial_z v + Kv - \frac{\beta_2}{2}\partial_t^2 v + \gamma(|v|^2 + A|u|^2 + Bu^2v^*) = ig\left(1 + \frac{1}{\omega_g^2}\partial_t^2\right)v, \tag{13}$$

where the field components u and v are normalized in such a way that the power is $\mathcal{P}=(|u|^2+|v|^2)$, K is the birefringence parameter, γ is the nonlinear coefficient, and A and B determine the strength of the cross-phase modulation and four-wave mixing. In a isotropic medium such as silica fiber, $A=2/3$ and $B=1/3$ [34]. β_2 is the group velocity dispersion, g the gain coefficient, and ω_g the spectral gain bandwidth.

The gain coefficient g is replaced using Eq. (11), in which g_0 is treated as a constant, since it relaxes at a slow rate (the relaxation time is 10 ms) with respect to the cavity round-trip (100 ns). We make use of the same perturbative approach as in [23–26]: We assume that the group velocity dispersion β_2, the nonlinearity γ, and the gain filtering $\rho = g_0/\omega_g^2$ modify the optical electric field only slightly on each cavity round-trip, as does the gain dynamics quantified by the parameter a. To account formally for this assumption, we introduce some small parameter ε and replace the parameters β_2, γ, ρ, and a with $\varepsilon\beta_2$, $\varepsilon\gamma$, $\varepsilon\rho$ and εa, respectively. Hence the small parameter ε is assumed to coincide with η of the previous section, which means that the effect of the fast component of the gain dynamics has the same order of magnitude as the nonlinear and dispersion effects. Although Eqs. (12) and (13) are written using the physical time t, they account for the same time scale as the scaled time T in the previous section.

The field components u and v are sought under the form of a power series of ε as

$$u = u_0 + \varepsilon u_1 + O(\varepsilon^2) \tag{14}$$

and analogously for v (below, we will systematically give the expression of u, while an analogous expression for v exists an will be omitted). At order ε^0 we get

$$u_0 = \tilde{u}_0 e^{(g_0 - iK)z}, \tag{15}$$

where $\tilde{u}_0$ is a function of t only. At order ε we get

$$\frac{\partial\tilde{u}_1}{\partial z} = \left(\rho - i\frac{\beta_2}{2}\right)\partial_t^2\tilde{u}_0 + i\gamma(\tilde{u}_0|\tilde{u}_0|^2 + A\tilde{u}_0|\tilde{v}_0|^2)e^{2g_0z} + i\gamma B\tilde{v}_0^2\tilde{u}_0^* e^{(2g_0+4iK)z} - g_0 a\tilde{u}_0\left[\int_{-\infty}^{t}(|\tilde{u}_0|^2 - \langle|\tilde{u}_0|^2\rangle + |\tilde{v}_0|^2 - \langle|\tilde{v}_0|^2\rangle)(t')dt'\right]e^{2g_0z}, \tag{16}$$

where we have set

$$u_1 = \tilde{u}_1(z,t)e^{(g_0 - iK)z}. \tag{17}$$

Equation (16) is integrated with respect to z; then, the whole field component u is reconstructed using

$$u(z,t) = [\tilde{u}_0(t) + \varepsilon\tilde{u}_1(z,t)]e^{(g_0 - iK)z} + O(\varepsilon^2), \tag{18}$$

for both the initial data $z=0$ and a nonzero value of z, to yield

$$u(z,t) = u(0,t)e^{(g_0 - iK)z} + \varepsilon\left\{ z\left(\rho - \frac{i\beta_2}{2}\right)\partial_t^2 u(0) + \left[i\gamma[u(0) \times |u(0)|^2 + Au(0)|v(0)|^2] - g_0 a u(0)\int_{-\infty}^{t} [|u(0)|^2 - \langle |u(0)|^2\rangle + |v(0)|^2 - \langle |v(0)|^2\rangle]dt' \right]\frac{e^{2g_0 z} - 1}{2g_0} + i\gamma B v(0)^2 u^*(0)\frac{e^{(2g_0 + 4iK)z} - 1}{2g_0 + 4iK}\right\} e^{(g_0 - iK)z} + O(\varepsilon^2), \tag{19}$$

and, as above, an analogous expression for the other component v.

B. Action of the polarizer

We denote by θ_- and θ_+ the angles between the fiber eigenaxis and the passing axes of the polarizer, before and after it, respectively. The corresponding field components are denoted by (u_-, v_-) and (u_+, v_+), respectively (cf. Fig. 6). The polarization of the optical field immediately after the polarizer is linear. We denote by f_n its amplitude at the beginning of the nth round-trip. The action of the polarizer can be expressed by

$$\begin{pmatrix} u_{+,n}(0) \\ v_{+,n}(0) \end{pmatrix} = f_n \begin{pmatrix} \cos\theta_+ \\ \sin\theta_+ \end{pmatrix}, \tag{20}$$

$$f_n = \Gamma(\cos\theta_- \sin\theta_-)\begin{pmatrix} u_{-,n-1}(L) \\ v_{-,n-1}(L) \end{pmatrix}, \tag{21}$$

where $(u_n, v_n)(z)$ are the field components during the nth round-trip, L is the fiber length, and $\Gamma < 1$ is the transmission coefficient of the polarizer.

C. Master equation

Here $u_n(L)$ is expressed as a function of $u_n(0)$ using Eq. (19), and analogously for v, which yields after some computation the expression of f_{n+1} as a function of f_n as

$$f_{n+1} = \Gamma e^{g_0 L}\left\{ Qf_n + \varepsilon\left[\left(\rho - \frac{i\beta_2}{2}\right)LQ\partial_t^2 f_n + iPf_n|f_n|^2 - Rg_0 a f_n \int_{-\infty}^{t} (|f_n|^2 - \langle |f_n|^2\rangle)dt' \right]\right\} + O(\varepsilon^2), \tag{22}$$

with

$$Q = \cos(\theta_+ - \theta_-)\cos KL - i\cos(\theta_+ + \theta_-)\sin KL, \tag{23}$$

$$P = \gamma\left\{ \frac{e^{2g_0 L} - 1}{2g_0}\left(Q + \frac{A-1}{2}\sin 2\theta_+ [\sin(\theta_+ + \theta_-)\cos KL - i\sin(\theta_+ - \theta_-)\sin KL]\right) + \frac{B}{2}\sin 2\theta_+ \left[\sin\theta_+ \cos\theta_- e^{-iKL}\frac{e^{(2g_0 + 4iK)L} - 1}{2g_0 + 4iK} + \cos\theta_+ \sin\theta_- e^{iKL}\frac{e^{(2g_0 - 4iK)L} - 1}{2g_0 - 4iK}\right]\right\}, \tag{24}$$

and

$$R = \frac{e^{2g_0 L} - 1}{2g_0}Q. \tag{25}$$

The gain threshold can be estimated as follows: the laser operates if the gain compensates the losses. The threshold corresponds to the limit of low amplitude of this condition. In the present formalism, it is written as $|f_{n+1}| = |f_n| + O(\varepsilon)$. Using Eq. (22), it yields $|\eta e^{g_0 L}Q| = 1 + O(\varepsilon)$; hence, $g_0 = g_0^L + \varepsilon g_1^L$, where g_1^L is some excess of gain, and

$$g_0^L = \frac{-1}{2L}\ln(\Gamma^2|Q|^2) = \frac{-1}{2L}\ln\{\Gamma^2[\cos^2(\theta_+ - \theta_-) - \sin 2\theta_+ \sin 2\theta_- \sin^2 KL]\}. \tag{26}$$

The above condition is inserted into Eq. (22), writing $\Gamma e^{g_0^L L}Q$ as a phase factor $e^{i\psi}$, to yield (from now on, the superscript L will be omitted)

$$f_{n+1} = e^{i\psi}(1 + \varepsilon g_1 L)f_n + \varepsilon\left(\rho - \frac{i\beta_2}{2}\right)Le^{i\psi}\partial_t^2 f_n + i\varepsilon\frac{Pe^{i\psi}}{Q}f_n|f_n|^2 - \varepsilon e^{i\psi}ag_0\frac{e^{2g_0 L} - 1}{2g_0}f_n\int_{-\infty}^{t}(|f_n|^2 - \langle |f_n|^2\rangle)dt' + O(\varepsilon^2). \tag{27}$$

A continuous evolution equation valid for a large number of round-trips is derived from the discrete evolution equation (27) using the procedure described in Ref. [23]. It involves a slow evolution variable $\xi = \varepsilon z$, so that

$$\partial_z = \partial_{\hat{z}} + \varepsilon\partial_\xi, \tag{28}$$

and fast evolution, which is only a linear phase factor, is set apart so that $f(z,t) = \mathcal{F}(\xi,t)\exp(i\psi\hat{z}/L)$. This yields the equation for $\mathcal{F}$ as

$$i\partial_\xi\mathcal{F} = ig_1\mathcal{F} + \left(\frac{\beta_2}{2} + i\rho\right)\partial_t^2\mathcal{F} + (\mathcal{D}_r + i\mathcal{D}_i)\mathcal{F}|\mathcal{F}|^2 - i\mathcal{G}\mathcal{F}\int_{-\infty}^{t}(|\mathcal{F}|^2 - \langle |\mathcal{F}|^2\rangle)dt', \tag{29}$$

with

$$\mathcal{D}_r + i\mathcal{D}_i = \frac{-P}{QL}, \tag{30}$$

$$\mathcal{G} = g_0 a \frac{e^{2g_0 L} - 1}{2g_0 L}. \tag{31}$$

After coming back to the laboratory values (without ε), the parameters β_2, γ, ρ, and a take their physical values again and ξ coincides with the distance z covered in the cavity and is assumed to take large values corresponding to large numbers of round-trips.

$\mathcal{D}_r$ and $\mathcal{D}_i$ are computed using Eqs. (23), (24), and (30). They depend on the orientation angles θ_+ and θ_-. It can be shown numerically that the effective self-phase modulation parameter $\mathcal{D}_r$ is always negative. $\mathcal{D}_i$ represents either an effective nonlinear gain or a loss depending on its sign. These parameters were already computed in Ref. [23], in contrast with $\mathcal{G}$, which is the gain modulation parameter.

Equation (29) is a cubic CGL equation [35], with an additional integral term which accounts for the fast component of the gain dynamics.

V. LOCAL STRUCTURE: A PERIODIC PULSE TRAIN

At the time scale accounted for by the above equations and within the approximations we have made, the experimental observation of a long pulse train corresponds to a periodical solution of Eq. (29). The goal of the present section is to prove that such a solution exists and has well-defined amplitude and period. Although an analytical localized pulse solution of Eq. (29) can be given (see below), the description of a periodical solution requires a numerical approach.

A. Numerical algorithm

We solve Eq. (29) by means of a standard fourth-order Runge-Kutta algorithm in Fourier space. The nonlinear terms are computed by applying the inverse Fourier transform [implemented through a standard fast Fourier transform (FFT) algorithm], computing the products in direct space, and applying again the direct FFT. Special attention must be paid to the integral term.

Let us denote by f_j, $j=0,\ldots,N-1$, a discrete variable representing some function $f(t)$ and F_k its discrete Fourier transform, defined by

$$F_k = \sum_{j=0}^{N-1} f_j e^{-(2i\pi/N)kj}, \tag{32}$$

$$f_j = \frac{1}{N} \sum_{k=0}^{N-1} F_k e^{(2i\pi/N)kj}. \tag{33}$$

It is well known that the inverse discrete Fourier transform (33) applied to $2i\pi k F_k$ gives a quite good approximation of the derivative $f'(t)$. Analogously, we consider $F_k^p = F_k/(2i\pi k)$ if $k \neq 0$ and $F_0^p = 0$, and construct its inverse Fourier transform f_j^p using (33). Let us denote by $f^p(t)$ the corresponding continuous function: its derivative is not exactly $f(t)$, but the continuous function whose discrete Fourier transform is F_k if $k \neq 0$, but 0 for $k=0$. Since F_0 is the mean value $\langle f \rangle$ of $f(t)$, $f^{p'}(t)$ is exactly $f(t) - \langle f \rangle$. Hence $f^p(t)$ is the antiderivative of $f(t) - \langle f \rangle$, which has a mean value zero. We use this property to compute the integral term in Eq. (29).

B. Formation of a periodic train

Equation (29) is solved numerically using the numerical algorithm presented above. We use as initial data the analytical soliton solution of the cubic CGL equation—i.e., of Eq. (29) with $\mathcal{G}=0$ [37]. Since the computations are very time consuming, the space of parameters is very large, and the results may depend crucially on the orientation angles, we make no attempt to obtain a quantitative agreement with the experiment. Therefore it is more convenient to use reduced dimensionless parameters. The change of variables,

$$\tau = \frac{t}{\sqrt{-\beta_2}}, \quad E = \mathcal{F}\sqrt{-\mathcal{D}_r}, \tag{34}$$

reduces Eq. (29) to

$$i\frac{\partial E}{\partial z} - i\delta E + \left(\frac{1}{2} - i\beta\right)\partial_\tau^2 E + (1 - i\epsilon)|E|^2 E + i\chi E \int^\tau (|E|^2 - \langle |E|^2 \rangle) d\tau' = 0, \tag{35}$$

with

$$\delta = g_1, \quad \beta = \frac{\rho}{-\beta_2}, \tag{36}$$

$$\epsilon = \frac{\mathcal{D}_i}{-\mathcal{D}_r}, \quad \chi = \frac{\mathcal{G}}{-\mathcal{D}_r}\sqrt{-\beta_2}. \tag{37}$$

If the integral term is omitted, Eq. (35) is the CGL equation in the reduced form used in Ref. [37] and in other works by the same authors. The reduction requires that both β_2 and $\mathcal{D}_r$ be negative, which is the case in our experiments. Notice that a further linear change allows us to set either δ or χ to an arbitrary value, with an adequate change in the value of the second of these parameters. Values of the coefficients for Eq. (29) can be computed from the expressions derived above. For the considered regime, we get typically $\beta = 7\times10^{-3}$, $\epsilon = 3\times10^{-3}$, and $\chi = 5\times10^{-4}$. Numerical computations show the appearance of a periodic pattern; however, the dynamics is very slow and cannot be analyzed in detail because of the excessive computation time required. Hence we replace these coefficients with larger, *ad hoc*, ones for which the dynamics is analogous, but the numerically study is achievable. We demonstrate that a periodic solution of this equation exists and has a well-defined peak amplitude, separation distance, and dephasing between pulses. We have checked that the *ad hoc* parameters can be effectively obtained by a suitable choice of the physical parameters.

For adequately chosen values of the parameters, and especially of the dimensionless gain saturation parameter χ, we observe the formation of a periodic solution from a single-input pulse. The corresponding evolution of the temporal distribution of the energy is given in Fig. 7. At the beginning of the process, a very irregular bunch of pulses arises [Figs. 7(a) and 7(b)]. Then a self-ordering of the pulse train occurs, simultaneously with its expansion to the whole computation

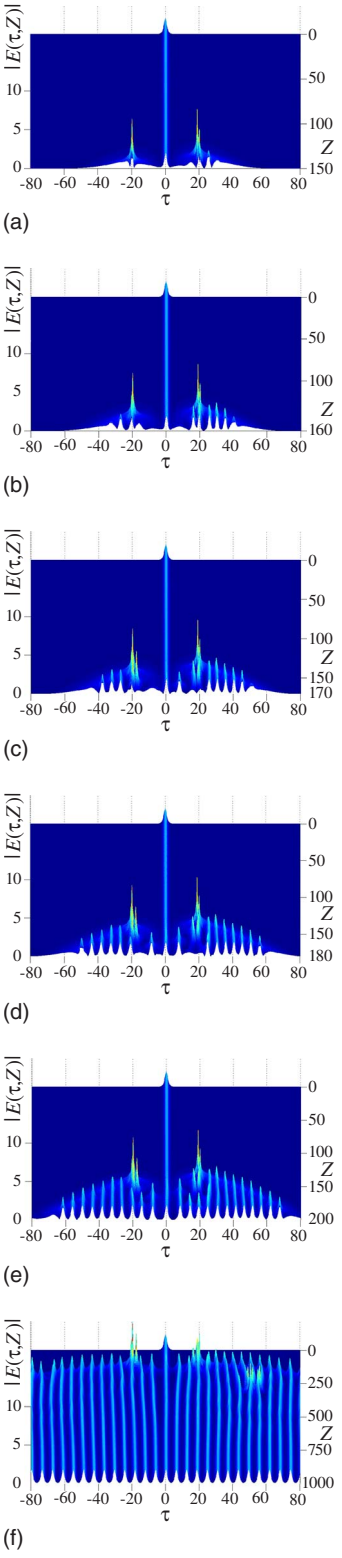

FIG. 7. (Color online) The evolution of the temporal profile of the intensity during propagation according to Eq. (29): A train of locked pulses is formed from an initial solitonlike input. (a) The single pulse generates two high-energy pulses. (b),(c) The high-energy pulses generate several pulses with various amplitudes and relative separation. (d),(e) The pulse train becomes more and more regular, and tends to fill the computation box. (f) A periodic solution is realized. Parameters: β=0.8, δ=0.1, ϵ=0.2, and χ=0.0009.

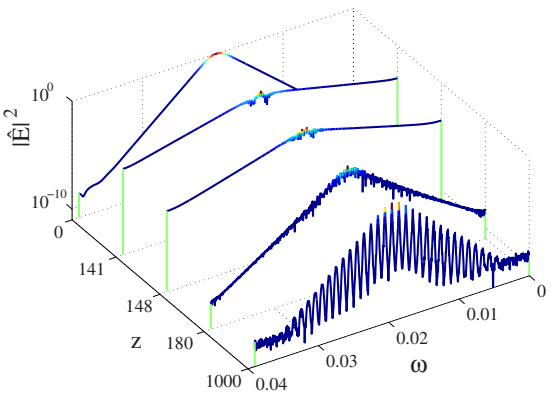

FIG. 8. (Color online) Evolution of the spectrum of the numerical solution (in logarithmic scale). A modulation of the initial pulse spectrum appears during the propagation, which shows the formation of a phase-locked periodic state.

box [Figs. 7(c)–7(e)]. During the evolution, their amplitudes, durations, and also the separation between them equilibrate mutually give rise to a train of identical, equidistant, and mutually locked pulses [Fig. 7(f)]. The evolution of the spectrum (Fig. 8) shows the appearance of a strong modulation, which accounts for the phase locking in the final periodic state.

C. Characteristics of the periodic solution

The final structure is stable and periodic, at least regarding the evolution of the amplitude. As stated above, the phase coherence of the pulse train can be seen from its spectrum, which presents a strong modulation (see Fig. 9).

The above computations show the existence and stability of a periodic solution to Eq. (29). Further, the pulse separation $\Delta\tau$ and the amplitude are determined by the parameters of the equation—i.e., physically by the laser parameters. This can be evidenced as follows: Figure 10 shows trajectories in the plane $(\max|E|^2, \Delta\tau)$—i.e., the evolution in a very large number of round-trips of the pulse separation versus the maximal amplitude of the electric field for several (nonperiodic) initial data. We observe that all curves reach the same point, which thus represents a stable, well-defined periodic solution. $\Delta\tau$ is computed as follows: first the pulse location is computed accurately by means of a parabolic interpolation of the numerical data. Then by subtraction we get the separations between all pairs of two consecutive pulses. $\Delta\tau$ is the mean value of these quantities for a given value of the propagation variable z.

Other computations have confirmed this observation; however, the stable periodic solution is not unique, but belongs to some discrete set of solutions. This is not surprising since multistability is common in fiber lasers [38].

VI. VARIATIONS OF GAIN AND FINITENESS OF THE TRAIN

A. Depletion of the gain

1. Expression of a localized pulse

An equation formally analogous to Eq. (29) has been derived in Ref. [36] in a slightly different context. An analytical

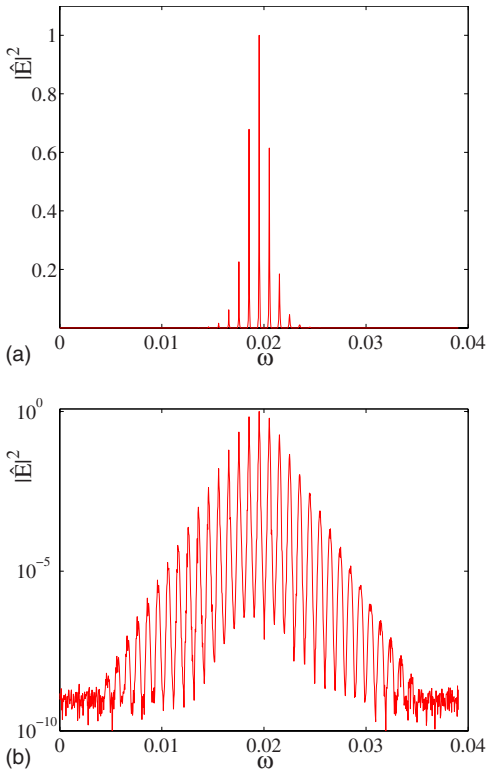

FIG. 9. (Color online) Spectrum of the numerical solution in linear (a) and logarithmic (b) scales. The strong modulation proves the phase locking between the pulses.

pulse solution was computed; let us recall it with the present notation. (If the reader intends to refer to the cited paper, he must avoid any confusion between the quantities denoted by D_r and D_i in Ref. [36] and the ones denoted by $\mathcal{D}_r$ and $\mathcal{D}_i$ here. There is no relation between them.) The first important point is to notice that, for a localized pulse, the mean value $\langle|\mathcal{F}|^2\rangle$ on the whole real line is zero. Then Eq. (29) admits the analytical solution

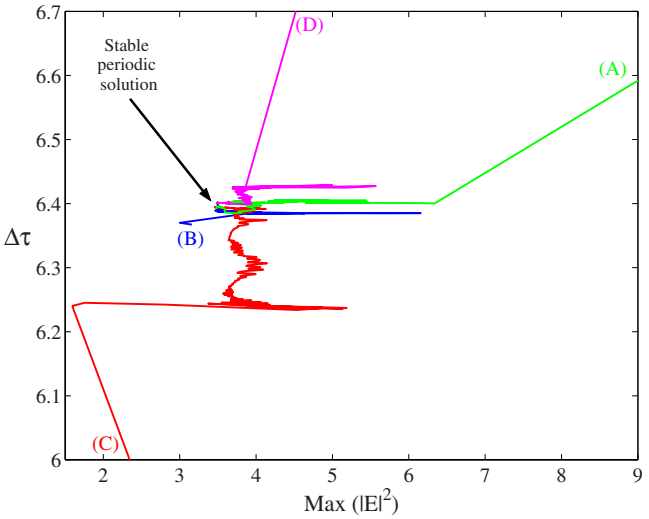

FIG. 10. (Color online) Average separation $\Delta\tau$ between two consecutive pulses versus the squared peak amplitude for several initial data. In every case, the solution converges to a stable periodic solution with the same determined amplitude and separation.

$$\mathcal{F} = \mathcal{F}_0 \frac{\exp i(\delta\omega t - \delta k z)}{\cosh^{1+i\alpha}[(t - wz)/\tau]}, \tag{38}$$

where τ is the pulse duration. w is the relative inverse pulse velocity, given by

$$w = -|\mathcal{F}_0|^2 \frac{\tau^2}{1+\alpha^2} \mathcal{G}\left(1 + \frac{\alpha\beta_2}{2\rho}\right). \tag{39}$$

The frequency shift $\delta\omega$ is

$$\delta\omega = \frac{-\alpha w}{\alpha\beta_2 + 2\rho}, \tag{40}$$

the correction δk to the wave number is

$$\delta k = \frac{-2\alpha\rho}{\tau^2} + \frac{\beta_2}{2}\left(\frac{1-\alpha^2}{\tau^2} - \delta\omega^2\right) \tag{41}$$

(note that a factor D_i is missing in the expression of δk in Ref. [36]), and the squared peak amplitude is

$$|\mathcal{F}_0|^2 = \frac{3\alpha}{\tau^2} \frac{(4\rho^2 + \beta_2^2)}{2(\beta_2\mathcal{D}_i - 2\rho\mathcal{D}_r)}. \tag{42}$$

The chirp parameter α satisfies the equation

$$\frac{\alpha}{2-\alpha^2} = \frac{\beta_2\mathcal{D}_i - 2\rho\mathcal{D}_r}{3(\beta_2\mathcal{D}_r + 2\rho\mathcal{D}_i)}. \tag{43}$$

2. Existence of the pulse solution

According to Eq. (42), the chirp parameter α must have the same sign as the quantity $\Xi = \beta_2\mathcal{D}_i - 2\rho\mathcal{D}_r$. Notice that Eq. (43) admits two solutions with opposite signs. Ξ can be computed numerically over the whole range of values of θ_+ and θ_- for values of the parameters corresponding to the experiment: group velocity dispersion $\beta_2 = -0.002$ ps^2/m, birefringence parameter $K = 1.5$ m^{-1}, nonlinear coefficient $\gamma = 3\times10^{-3}$ W^{-1} m^{-1}, and spectral gain bandwidth $\omega_g = 15.7$ ps^{-1}. It is seen that Ξ is always positive. Hence the chirp parameter α is given by the positive solution of Eq. (43). Figure 11 illustrates the evolution of α versus the orientation angles θ_+ and θ_-.

As does α, the product $|\mathcal{F}_0|^2\tau^2 = \Phi$ given by Eq. (42) depends on the cavity parameters mentioned above only. Hence the frequency shift $\delta\omega$ can be expressed as

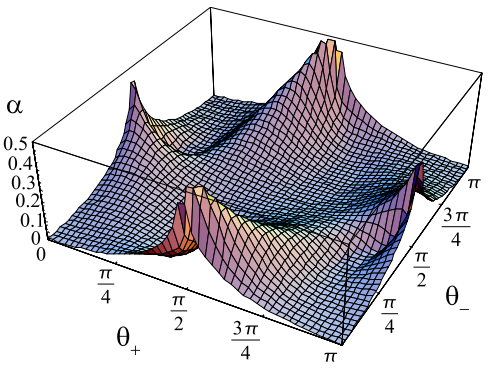

FIG. 11. (Color online) The frequency chirp α as a function of the orientation angles θ_+ and θ_- of the phase plates.

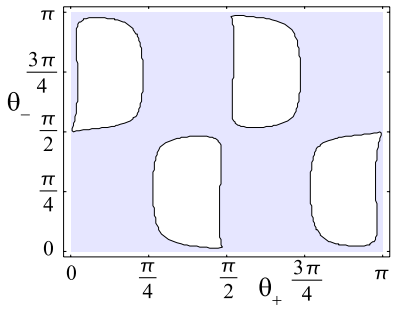

FIG. 12. (Color online) The sign of the quantity $\mathcal{H}$ versus the angles θ_+ and θ_-: The analytic pulse exists above some threshold of excess gain for $\mathcal{H}<0$ (gray regions).

$$\delta\omega = \frac{\Phi\alpha\mathcal{G}}{2(1+\alpha^2)\rho}. \tag{44}$$

The pulse duration τ must satisfy the quadratic polynomial equation

$$(g_1 - \rho\delta\omega^2)\tau^2 - \mathcal{G}\Phi\tau + [(1-\alpha^2)\rho + \alpha\beta_2] = 0. \tag{45}$$

The analytical solution (38) exists if Eq. (45) admits a real solution—i.e., if Δ is positive, with

$$\Delta = \mathcal{G}^2\Phi^2 - 4\mathcal{H}(g_1 - \rho\delta\omega^2), \tag{46}$$

where

$$\mathcal{H} = [(1-\alpha^2)\rho + \alpha\beta_2]. \tag{47}$$

The analytical solution (38) exists for an excess of gain g_1 either below or above some threshold g_{1th}, depending on the sign of $\mathcal{H}$. Since the existence of an upper gain threshold (i.e., the condition $g_1 < g_{1th}$) appears as an unphysical case, we require that $\mathcal{H}<0$, and solution (38) exists for $g_1 > g_{1th}$, with

$$g_{1th} = \frac{\mathcal{G}^2\Phi^2}{4\mathcal{H}} + \rho\,\delta\omega^2. \tag{48}$$

The quantities $\mathcal{H}$ and $\Phi = |\mathcal{F}_0|^2\tau^2$ can be computed as functions of θ_+ and θ_-; the sign of $\mathcal{H}$ is shown in Fig. 12, and the value of Φ is drawn in Fig. 13. The threshold is always negative, and for typical values (precisely, the values corresponding to the first column of Table I below), we get $g_{1th} \sim -11.6\times10^{-6}$ m^{-1}. It will be seen that the gain depletion δg induced by the pulse has the same order of magnitude as this value (in fact, $\delta g / g_{1th}$ is very close to -2 for all values of parameters considered).

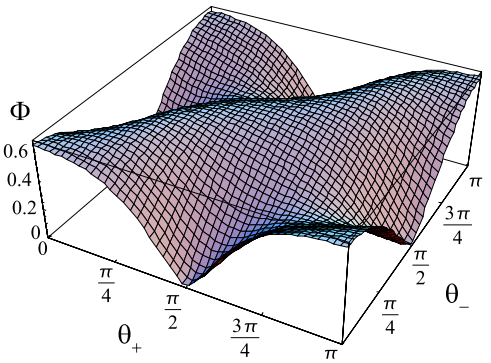

FIG. 13. (Color online) The product $\Phi = |\mathcal{F}_0|^2\tau^2$ of the squared peak amplitude times the squared pulse duration (in W ps^2), versus the orientation angles θ_+ and θ_-.

The duration of the pulses is estimated by the duration of the analytical pulse at the gain threshold g_{1th}, or $\Delta=0$. According to Eq. (45), it yields the value

$$\tau = \frac{2\mathcal{H}}{\mathcal{G}\Phi}, \tag{49}$$

which is plotted versus the orientation angles in Fig. 14.

Considering, e.g., orientation angles as $\theta_+=0.1$ rad and $\theta_-=0.1$ rad, we get a pulse duration of about 825 fs, in accordance with our experimental results. For the same parameters we check that $\mathcal{H}<0$, which ensures the existence of the analytical pulse solution above the threshold.

3. Depletion of gain

According to Eqs. (11) and (29), the depletion δg of the gain due to the isolated pulse is given by

$$\delta g = \mathcal{G}\int_{-\infty}^{+\infty} |\mathcal{F}(t)|^2 dt = 2\mathcal{G}|\mathcal{F}_0|^2\tau. \tag{50}$$

This value was already obtained in Ref. [36] (it is denoted there by $2\delta G$).

B. Gain relaxation

Between two pulse trains, the fast variations of gain are absent, and hence it relaxes, according to the slow evolution equation (8), in fact, more exactly according to the original equation (2), with $\mathcal{P}=0$. This equation is solved as

$$g(t) = g(0)e^{-t/\tau_g} + \Lambda\tau_g(1 - e^{-t/\tau_g}). \tag{51}$$

The variation Δg of the gain in the time interval ΔT separating two pulse trains (cf. Fig. 5) is thus

TABLE I. Numerical values for many choices of the orientation angles θ_+ and θ_-.

(θ_+, θ_-) (rad)	(0.1, 0.1)	(0.1, 0.2)	(3, 1.7)	(2, 1)	(2.9, 2.9)	(2.5, 3)	(1.7, 1.5)
τ (ps)	0.825	1.11	0.839	1.72	1.91	0.657	0.730
δg (m^{-1})	22.8×10^{-6}	20×10^{-6}	79.72×10^{-5}	87.52×10^{-6}	14.25×10^{-6}	13.24×10^{-5}	30.47×10^{-6}
Δg (m^{-1})	7.73×10^{-3}	7.73×10^{-3}	7.73×10^{-3}	7.73×10^{-3}	7.73×10^{-3}	7.73×10^{-3}	7.73×10^{-3}
$\Delta g / \delta g$	340	386	10	88	542	58	253

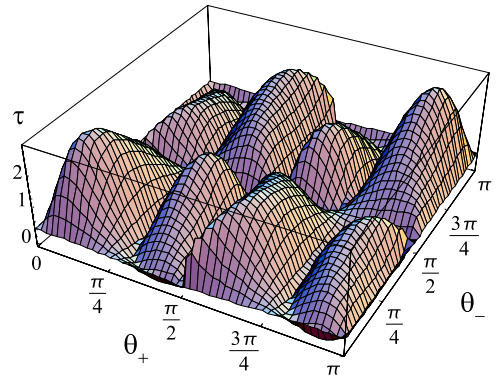

FIG. 14. (Color online) The pulse duration τ (in ps) versus the angles θ_+ and θ_-.

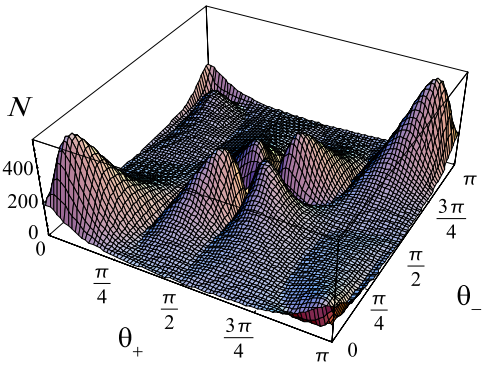

FIG. 15. (Color online) The number N of pulses in the train versus the angles θ_+ and θ_-.

$$\Delta g = (\Lambda \tau_g - g_i)(1 - e^{-\Delta T/\tau_g}). \tag{52}$$

Since $\Delta T/\tau_g \simeq 100$ ns/10 ms is small, expression (52) can be approximated by

$$\Delta g \simeq \Lambda \, \Delta T. \tag{53}$$

The cross section can be estimated as $\sigma = 5 \times 10^{-25}$ m^2 [30], and according to experiment, we can take $\Delta T = 100$ ns. This way we obtain the gain recovered in the absence of laser pulse (53): $\Delta g \approx 7.73 \times 10^{-3}$ m^{-1}.

Table I gives several examples of computations for suitable values of the angles θ_+ and θ_-. For the first choice of orientation angles, we get pulses with a duration of 825 fs. The gain depletion consecutive to a single pulse is $\delta g = 22.8 \times 10^{-6}$ m^{-1}. For a train containing $N = 340$ pulses, the total decrease of gain is $N\delta g \simeq 7.75 \times 10^{-3}$ m^{-1}. The gain recovered due to relaxation and pumping in the time interval between two consecutive passes of the pulse train is $\Delta g \approx 7.73 \times 10^{-3}$ m^{-1}. The pumping thus exactly compensates the gain depletion due to the pass of the pulse train at each round-trip. The obtained value of the number N of pulses is in good agreement with experiment, which confirms the validity of the interpretation. Using the same procedure, N can be computed as a function of the orientation angles of the phase plates; see Fig. 15. In our analysis we assume that the length of the soliton train is small with respect to the cavity length. Within this approximation, the upper value g_m of the gain is expected to be independent of the pumping, equal to the gain at the laser threshold, estimated by g_0. As each pulse goes through the cavity, the gain is depleted by δg and decreases until the minimal value $g_m - N\delta g$, for which the gain g_m can be recovered during the remaining of the round-trip, is reached.

VII. CONCLUSION

Trains of bounded short pulses have been observed in a fiber laser. They form a quasiperiodic pattern in the sense that the local structure is periodic, while the train has a finite length. We explained it theoretically by considering separately the two characteristic time scales of the process.

The local structure, corresponding to the formation of a periodic pattern, which locally compares to a soliton crystal, is governed by the fast time scale. The slow time accounts for the delimitation of a pulse train of definite length, which makes it rather comparable to a macromolecule. From the theoretical point of view, the separation of the two scales was allowed by the multiscale analysis. It must be noticed that in the experiment, also, the separation of the two time scales occurs. Indeed, their observation requires different measurement procedures: autocorrelation for the fast scale and oscilloscope for the slow one.

Then both small- and large-scale phenomena are accounted for by the theoretical analysis. The local periodical pattern formation has been described numerically by means of a CGL-type model including the fast gain dynamics. The gain depletion involved by each pulse was estimated by means of an analytical solution of this equation and compared to the gain recovered by relaxation. The finiteness of the wave train is thus explained through a conservation law: the number of pulses in the steady state is such that the decrease of gain due to the amplification of each pulse can be compensated for by the pumping.

ACKNOWLEDGMENTS

This work has been partially financed by the European Community (FEDER). It is also supported by a Marie Curie program within the 6th European Community Framework Program (Grant No. 039942-PMLFL).

[1] V. V. Afanasjev, B. A. Malomed, and P. L. Chu, Phys. Rev. E **56**, 6020 (1997).
[2] N. N. Akhmediev, A. Ankiewicz, and J. M. Soto-Crespo, Phys. Rev. Lett. **79**, 4047 (1997).
[3] N. N. Akhmediev, A. Ankiewicz, and J. M. Soto-Crespo, J. Opt. Soc. Am. B **15**, 515 (1998).
[4] D. Y. Tang, W. S. Man, H. Y. Tam, and P. D. Drummond, Phys. Rev. A **64**, 033814 (2001).
[5] Ph. Grelu, F. Belhache, F. Gutty, and J.-M. Soto-Crespo, Opt. Lett. **27**, 966 (2002).
[6] A. Hideur, B. Ortaç, T. Chartier, M. Brunel, H. Leblond, and F. Sanchez, Opt. Commun. **225**, 71 (2003).
[7] H. Leblond, A. Komarov, M. Salhi, A. Haboucha, and F. Sanchez, J. Opt. A, Pure Appl. Opt. **8**, 319 (2006).
[8] Ph. Grelu and J.-M. Soto-Crespo, J. Opt. B: Quantum Semiclassical Opt. **6**, S271 (2004).
[9] B. Ortaç, A. Hideur, T. Chartier, M. Brunel, Ph. Grelu, H. Leblond, and F. Sanchez, IEEE Photonics Technol. Lett. **16**, 1274 (2004).
[10] D. Y. Tang, L. M. Zhao, and B. Zhao, Appl. Phys. B: Lasers Opt. **80**, 239 (2005).
[11] Ph. Grelu, F. Belhache, F. Gutty, and J.-M. Soto-Crespo, J. Opt. Soc. Am. B **20**, 863 (2003).
[12] E. Fermi, J. Pasta, and H. C. Ulam, in *Collected Papers of Enrico Fermi*, edited by E. Segrè (The University of Chicago, Chicago, 1965), Vol. 2, pp. 977–988.
[13] N. N. Akhmediev, V. M. Eleonskii, and N. E. Kulagin, Sov. Phys. JETP **62**, 894 (1985).
[14] C. Cambournac, H. Maillotte, E. Lantz, J. M. Dudley, and M. Chauvet, J. Opt. Soc. Am. B **19**, 574 (2002).
[15] K. Tai, A. Hasegawa, and A. Tomita, Phys. Rev. Lett. **56**, 135 (1986).
[16] E. M. Dianov, P. V. Mamyshev, A. M. Prokhorov, and S. V. Chernikov, Opt. Lett. **14**, 1008 (1989).
[17] S. Rutz and F. Mitschke, J. Opt. B: Quantum Semiclassical Opt. **2**, 364 (2000).
[18] B. A. Malomed, A. Schwache, and F. Mitschke, Fiber Integr. Opt. **17**, 267 (1998).
[19] P. Franco, F. Fontana, I. Cristiani, M. Midrio, and M. Romagnoli, Opt. Lett. **20**, 2009 (1995).
[20] E. Yoshida and M. Nakazawa, Opt. Lett. **22**, 1409 (1997).
[21] T. Sylvestre, S. Coen, Ph. Emplit, and M. Haelterman, Opt. Commun. **247**, 181 (2005).
[22] A. Haboucha, H. Leblond, M. Salhi, A. Komarov, and F. Sanchez, Opt. Lett. **33**, 524 (2008).
[23] H. Leblond, M. Salhi, A. Hideur, T. Chartier, M. Brunel, and F. Sanchez, Phys. Rev. A **65**, 063811 (2002).
[24] M. Salhi, H. Leblond, and F. Sanchez, Phys. Rev. A **67**, 013802 (2003).
[25] M. Salhi, H. Leblond, and F. Sanchez, Phys. Rev. A **68**, 033815 (2003).
[26] M. Salhi, A. Haboucha, H. Leblond, and F. Sanchez, Phys. Rev. A **77**, 033828 (2008).
[27] M. Salhi, H. Leblond, and F. Sanchez, Opt. Commun. **247**, 181 (2005).
[28] A. Hideur, T. Chartier, M. Salhi, C. Ozkul, C. Brunel, and F. Sanchez, Opt. Commun. **198**, 141 (2001).
[29] A. Komarov, H. Leblond, and F. Sanchez, Phys. Rev. A **72**, 063811 (2005).
[30] Michel J. F. Digonnet, *Rare-Earth-Doped Fiber Lasers and Amplifiers*, 2nd ed. (Marcel Dekker, New York, 2001).
[31] O. Svelto, *Principles of Lasers* (Springer, Berlin, 1998).
[32] H. Leblond, J. Phys. B **41**, 043001 (2008).
[33] A. D. Kim, J. N. Kutz, and D. J. Muraki, IEEE J. Quantum Electron. **36**, 465 (2000).
[34] G. P. Agrawal, *Nonlinear Fiber Optics* (Academic Press, San Diego, 1995).
[35] I. S. Aranson and L. Kramer, Rev. Mod. Phys. **74**, 99 (2002).
[36] A. Komarov, H. Leblond, and F. Sanchez, Opt. Commun. **267**, 162 (2006).
[37] N. N. Akhmediev and A. Ankiewics, *Solitons, Nonlinear Pulses and Beams* (Chapman-Hall, London, 1997).
[38] A. Komarov, H. Leblond, and F. Sanchez, Phys. Rev. A **71**, 053809 (2005).